The following publication T. Kauffmann et al., "Short-Circuit Model for Type-IV Wind Turbine Generators With Decoupled Sequence Control," in IEEE Transactions on Power Delivery, vol. 34, no. 5, pp. 1998-2007, Oct. 2019 is available at https://dx.doi.org/10.1109/TPWRD.2019.2908686.

Short-Circuit Model for Type-IV Wind Turbine Generators with Decoupled Sequence Control

T. Kauffmann, *IEEE Student Member,* U. Karaagac, *IEEE Member*, I. Kocar, *IEEE Senior Member*, S. Jensen, E. Farantatos, *IEEE Member,* A. Haddadi, *IEEE Member*, J. Mahseredjian, *IEEE Fellow*

***Abstract*— The power system planning and protection studies are becoming more challenging due to the rapid increase in penetration levels of converter-interfaced renewables. Type-IV wind turbine generators (WTGs) and photovoltaic panels (PVs) are interfaced to the grid through a full-scale converter (FSC), and their short-circuit current contributions are mainly designated by the converter control and associated current limits. This paper proposes a new phasor domain modeling approach for the wind parks (WPs) with Type-IV WTGs using the concept of control-based equivalent circuits. The proposed model precisely represents the detailed electromagnetic transient type (EMT-type) model in steady state and is able to account for the fault-ride-through (FRT) function of the WTG control as well as its specific decoupled sequence control scheme in addition to the traditional coupled control scheme. Although the collector grid and WTGs inside the WP are represented with their aggregated models, the overall reactive power control structure of the WP is preserved by taking the central wind park controller (WPC) into account. The accuracy of the proposed model is validated through detailed EMT simulations.**

***Index Terms*— Full-scale converter (FSC), phasor domain modeling, protection studies, short-circuit calculation, unbalanced faults, wind turbine generators.**

I. Introduction

The short-circuit behavior of the electronically coupled generators (ECGs) can be studied with high precision using electromagnetic transient (EMT) simulation tools [1]-[4]. On the other hand, the short-circuit analysis packages are traditionally used for protection studies. In short circuit packages, ECGs are often modeled as either conventional synchronous machines (voltage source behind an impedance) or a current source to limit the short circuit current contribution to a user defined level (e.g. 1.2 pu). These models disregard the complex characteristics of the ECG converter controls. The existing literature contains limited number of solutions for phasor domain modeling of ECGs. This paper focuses on phasor domain modeling of Type-IV WTG based wind parks (WPs) for short-circuit analysis and protection packages.

In [5], a small-scale distribution level Type-IV WTG is represented with a controlled current source that adjusts its output current to deliver the pre-fault active power while accounting for the grid side converter (GSC) current limits. However, this model cannot be used for large-scale transmission level Type-IV WTG based WPs as majority of the grid codes (such as [6]) impose a fault-ride-through (FRT) requirement to support the grid voltage during faults.

In [7], the Type-IV WTG is also represented by a controlled current source in which the active power component of the GSC current is set to its pre-fault value and reactive power component is increased up to the GSC current limit. The drawback is that the WTG fault current contribution is same for any fault condition for a given pre-fault active power generation.

In [8], the Type-IV WTG is represented with a constant voltage source behind a variable impedance. The variable impedance is adjusted considering the GSC current limit through an iterative solution. However, the response of the GSC control to the voltage sag is disregarded (except its current limit).

The phasor domain model of Type-IV WTG in [9] is based on controllable equivalent circuits and accounts for the outer control loop of the GSC and FRT function through an iterative loop solution. This model is improved further in [10] by considering a realistic WP reactive power control structure that includes the WP controller (WPC). On the other hand, the usage of this model is limited to the traditional coupled sequence control (CSC) scheme.

Ideally, the GSC with CSC is not expected to inject any negative sequence currents to the grid during unbalanced loading conditions or faults. In practice, it injects a very small amount due to the phase shift in low pass measuring filters [10]. As discussed in [11]-[13], lack of negative sequence fault current contribution from the Type-IV WTG may cause misoperation of protection system during certain unbalanced fault conditions. Unlike its output currents, the GSC terminal voltages contain negative sequence component during unbalanced loading conditions or faults, and this causes second harmonic oscillations in the GSC active power output as well as the dc bus capacitor voltage. These second harmonic oscillations can be eliminated by adopting a decoupled sequence control (DSC) scheme [14]. During faults, if the priority is injecting the positive sequence reactive currents designated by the FRT requirement, then the second harmonic

T. Kauffmann, I. Kocar, A. Haddadi and J. Mahseredjian are with Polytechnique Montréal, Montréal, (Québec), Canada; U. Karaagac is with The Hong Kong Polytechnic University, Hong Kong, China; S. Jensen is with Siemens SE, Hamburg, Germany; E. Farantatos is with EPRI, CA, USA.

oscillation mitigation performance of the DSC will be limited by the unbalanced fault type, fault location as well as the GSC current limit [15]. The GSC operating under DSC also injects considerable amount of negative sequence currents during unbalanced faults (depending on its type and location). Hence, the possibility of protection system misoperation is expected to be less compared to the GSC operating under CSC.

This paper contributes a steady-state modeling approach for Type-IV WTG based WP. The proposed model is a controlled equivalent circuit, and as demonstrated it can precisely represent the detailed EMT model in steady state. It accounts for the outer control loop of GSC, the DSC scheme of the EMT model and the FRT function through an iterative solution. The proposed model considers the WP reactive power control structure in [10],[15],[16] and takes the WPC into account. The model is added into a modified augmented nodal analysis (MANA) based multiphase short circuit solver [17], [18]. The proposed model is validated through EMT simulations. The implementation details of the detailed generic EMT model is documented in [15], which is provided with this paper as a supporting document. The EMT model has been validated against fault records and manufacturers DLL model for short circuit studies [19]-[21]. Depending on the manufacturer and grid code requirements, it is possible to have different control schemes. The proposed modeling approach has the ability to represent Type-IV WTGs with different control schemes. The negative sequence reactive current scheme of the recent German VDE-AR-N 4120 Technical Connection Rules [22] is also considered to show how the steady-state methodology can be adapted to different control schemes.

The main contribution of this paper is a flexible modelling approach for the WPs with Type-IV WTGs which is able to account for different advanced control schemes and transient functions. The proposed approach can be used to represent Type-IV WTGs with arbitrary DSC schemes and/or FRT functions. To the authors' best knowledge such advanced control schemes and transient functions have be disregarded in exiting literature. The proposed approach can be used in professional short-circuit packages to build a library for full scale-converter (FSC) interfaced renewables with different control schemes. Ability to predict accurate negative sequence fault current contributions of FSC interfaced renewables will ensure proper protection system design for power systems with high renewable penetration levels.

The first part presents WPs with Type-IV WTGs. The proposed phasor domain model and solution algorithm are presented in the second part. The last part presents the simulation results.

II. Wind Parks with Type-IV Wind Turbine Generators

In a typical WP, the power produced by the WTGs are transmitted to the point of interconnection (POI) through a medium voltage collector grid and a WP transformer as shown in Fig. 1. Although not shown in Fig. 1, the WP transformer usually has an on-load-tap-changer to keep the MV collector bus voltage around its nominal value. According to customary grid code requirements, the WP should have a central WPC at the WP substation to control the reactive power, voltage or power factor at the POI.

This section briefly presents Type-IV WTGs and reactive power control in WPs that will be useful in building phasor model. The implementation details of the presented WTG is given in [15].

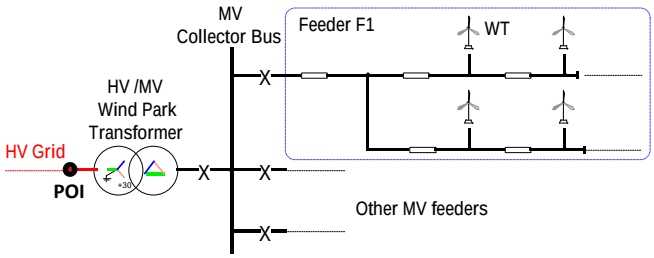

Fig. 1. Simplified single-line diagram of a typical wind park.

A. Type-IV Wind Turbines

A Type-IV WTG may employ a wide range of electrical generators such as induction generator, conventional synchronous generator and permanent magnet synchronous generator (PMSG). As all the WTG power is transferred through an ac-dc-ac converter system, the specific characteristics and dynamics of the electrical generator are effectively isolated from the grid [23]. The considered topology uses a PMSG and a converter system consists of two pulse-width modulated voltage source converters.

As shown in Fig. 2, the grid side converter (GSC) has a two-stage controller. The slow outer control calculates the reference dq-frame currents and the fast inner (current) control produces the converter ac voltage reference. The GSC operates in the voltage reference frame. d-axis current of GSC (i_{dg}) is used to control dc bus voltage (V_{dc}). q-axis current of GSC (i_{qg}) is used to control the positive sequence terminal voltage of GSC ($\left|\bar{V}_g^+\right|$). The reference for GSC positive sequence terminal voltage (V') is adjusted by the WPC to achieve the desired reactive power at the POI. The sequence components are extracted through the decoupled PLL detailed in [27].

On the other hand, the machine side converter (MSC) operates at unity power factor and controls the PMSG torque to follow the reference given by the MPPT algorithm for optimal power generation depending on wind speed.

During normal operation, the priority is given to the active power component of the GSC currents, i.e.

$$\begin{aligned} i'_{dg} &< I_{dg}^{\lim} && , I_{dg}^{\lim} = 1\ pu \\ i'_{qg} &< I_{qg}^{\lim} = \sqrt{\left(I_g^{\lim}\right)^2 - \left(i'_{dg}\right)^2} && , I_g^{\lim} = 1.1\ pu \end{aligned} \quad (1)$$

where $I_g^{\lim}$ is the GSC current limit.

In this section and hereinafter, all variables are in pu (unless stated otherwise) and primed variables are used to indicate the reference values coming from the controllers. The plus and minus signs ("+" and "-") indicate positive and negative sequence components, respectively.

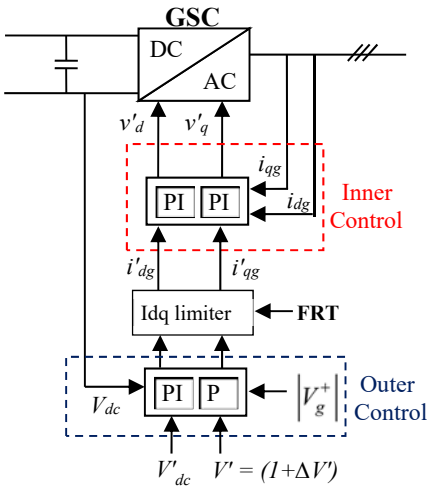

Fig. 2. Schematic diagram of GSC coupled sequence control.

B. Fault-Ride-Through (FRT) Function

The grid code requirements, such as [6], include the WTG transient response against severe voltage disturbances (see Fig. 3 for the additional reactive current requirement versus voltage change in the positive sequence system). To comply with this requirement, an FRT function is traditionally added to the GSC control. The FRT function activates when $|\left|\bar{V}_{mv}^{+}\right|-1|>V_{FRT-ON}$ and it deactivates when $|\left|\bar{V}_{mv}^{+}\right|-1|<V_{FRT-OFF}$ after a pre-specified release time t_{FRT}. $\left|\bar{V}_{mv}^{+}\right|$ is the magnitude of the positive sequence voltage of the WTG step-up transformer MV terminal, and it is estimated by the GSC control using the measured GSC terminal voltages and currents. During FRT operation, the GSC controller gives priority to the reactive current by reversing the d- and q-axis current limits given in (1) . In the recent VDE-AR-N 4120 Technical Connection Rules [22], there is also a required additional negative sequence reactive current as a function of the voltage change in the negative sequence system as shown in Fig. 4. This will be also studied in this paper as an alternative DSC scheme.

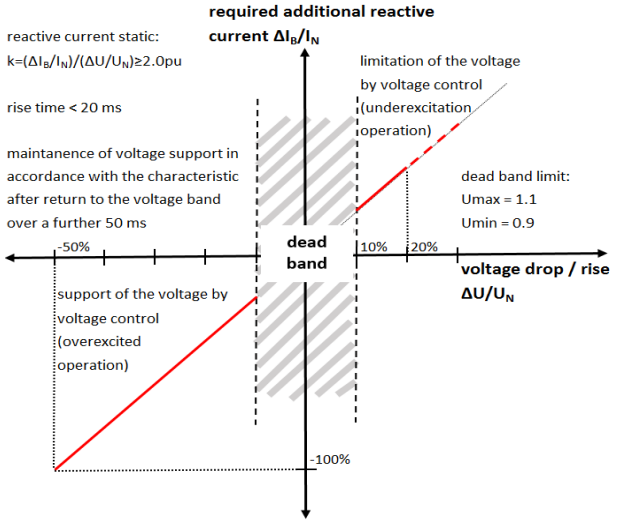

Fig. 3. Wind turbine reactive output current during voltage disturbances [6].

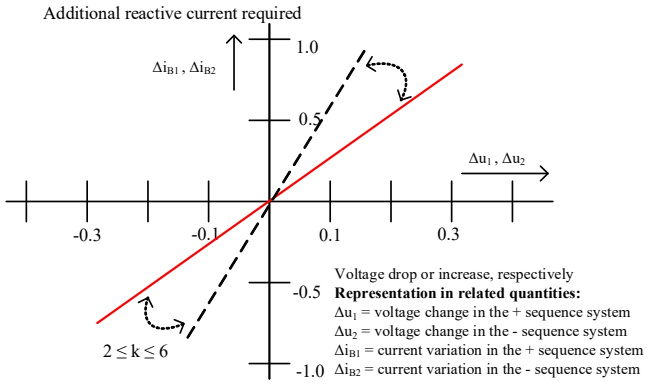

Fig. 4. Wind turbine reactive output current during voltage disturbances [22].

C. Grid Side Converter Decoupled Sequence Control

Ideally, the GSC control presented in the previous section is not expected to inject any negative sequence currents to the grid during unbalanced loading conditions or faults. On the other hand, its terminal voltage contains negative sequence components. The instantaneous active and reactive powers for such unbalanced grid conditions can be written as [14]:

$$\begin{aligned} p(t) &= P_0 + P_{C2}\cos(2\omega t) + P_{S2}\sin(2\omega t) \\ q(t) &= Q_0 + Q_{C2}\cos(2\omega t) + Q_{S2}\sin(2\omega t) \end{aligned} \quad (2)$$

where P_0 and Q_0 are the average values of the instantaneous active and reactive powers respectively, whereas P_{C2}, P_{S2}, Q_{C2} and Q_{S2} represent the magnitudes of the second harmonic oscillating terms in these instantaneous powers.

The oscillating terms in active power P_{C2}, P_{S2} cause oscillations in dc bus voltage V_{dc}. The first DSC scheme considered in this paper calculates GSC current references ($i_{dg}^{+\prime}$, $i_{qg}^{+\prime}$, $i_{dg}^{-\prime}$ and $i_{qg}^{-\prime}$) to control P_0 and Q_0, and cancel out P_{C2} and P_{S2} (i.e. $P_{C2}=P_{S2}=0$) [14] without considering the reactive current scheme in Fig. 4. The scheme in Fig. 4 is also implemented as an alternative DSC scheme but its equations are given only in the phasor domain in the next section since the relation is straightforward.

The GSC decoupled sequence control implementation in [15] keeps the outer control and Idq limiter shown in Fig. 2 to calculate i'_{dg}, i'_{qg}, $I_{dg}^{\lim}$ and $I_{qg}^{\lim}$. These values are used to calculate the GSC current references $i_{dg}^{+\prime}$, $i_{qg}^{+\prime}$, $i_{dg}^{-\prime}$ and $i_{qg}^{-\prime}$ for the decoupled sequence current controller. As the positive sequence reactive current injection during faults is defined by the grid code (see Fig. 3), the GSC current reference is calculated as below.

$$\begin{bmatrix} i_{qg}^{+\prime} \\ i_{dg}^{+\prime} \\ i_{qg}^{-\prime} \\ i_{dg}^{-\prime} \end{bmatrix} = \begin{bmatrix} 1 & 0 & 0 & 0 \\ v_{qg}^{+} & v_{dg}^{+} & v_{qg}^{-} & v_{dg}^{-} \\ v_{qg}^{-} & v_{dg}^{-} & v_{qg}^{+} & v_{dg}^{+} \\ -v_{dg}^{-} & v_{qg}^{-} & v_{dg}^{+} & -v_{qg}^{+} \end{bmatrix}^{-1} \begin{bmatrix} i'_{qg} \\ P_0 \\ P_{C2} \\ P_{S2} \end{bmatrix} \quad (3)$$

where P_0 is approximated by $P_0 = \left|V_g^+\right| i'_{dg}$

To respect the GSC current limit $I_g^{\lim}$, both positive and negative sequence components are reduced according to their proportion. For example when $\left(i_{qg}^{+\prime} + i_{qg}^{-\prime}\right) > I_{qg}^{\lim}$, the q-axis current references are revised as below:

$$\begin{aligned} i_{qg}^{+\prime\prime} &= i_{qg}^{+\prime}\left[I_{qg}^{\lim} \Big/ \left(i_{qg}^{+\prime} + i_{qg}^{-\prime}\right)\right] \\ i_{qg}^{-\prime\prime} &= i_{qg}^{-\prime}\left[I_{qg}^{\lim} \Big/ \left(i_{qg}^{+\prime} + i_{qg}^{-\prime}\right)\right] \end{aligned} \tag{4}$$

where $i_{qg}^{+\prime\prime}$ and $i_{qg}^{-\prime\prime}$ are the revised reference currents for q-axis. $I_{dg}^{\lim}$ and $I_{qg}^{\lim}$ are obtained with the current limiter presented in section II.A.

The revised d-axis reference currents are also calculated using the same approach. The schematic diagram of GSC DSC is shown in Fig. 5.

During faults, if there is no specific requirement for additional negative sequence reactive current as stipulated in [22] and shown in Fig. 4, the priority is providing i_{qg}^{+} specified by the grid code. The remaining reserve in GSC is used for delivering active power to grid (P_0) while eliminating the oscillating terms in active power (P_{C2} and P_{S2}).

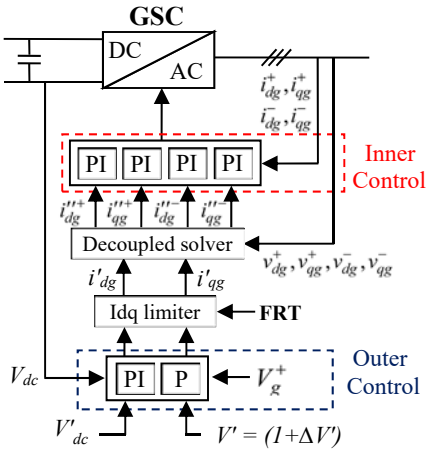

Fig. 5. Schematic diagram of GSC decoupled sequence control.

D. Reactive Power Control in Wind Parks

The reactive power at the POI is controlled using two control levels [24]. At primary level, the GSC controller controls its terminal voltage ($\left|V_g^+\right|$) with a proportional voltage regulator as explained above (see Fig. 2 and Fig. 5). At secondary level, the WPC controls the reactive power at the POI (Q_{POI}) by modifying the GSC controller reference voltage values (V') through a proportional-integral (PI) reactive power regulator (see Fig. 6).

While operating under Q-control function, the WPC receives reactive power reference Q'_{POI}. While operating under V-control function, Q'_{POI} is calculated by an outer proportional voltage control for the voltage reference V'_{POI}. Although not shown in Fig. 6, the WPC may contain a power factor control function in which Q'_{POI} is calculated using the measured active power at the POI and the desired power factor at the POI. This paper considers the WPC operating under Q-control.

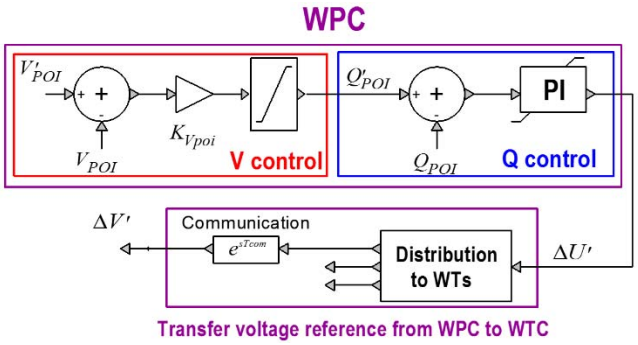

Fig. 6. Reactive power / voltage control at the point of interconnection (POI).

III. Phasor Model

In steady-state, the dq components of the positive and negative sequence currents and voltages contain only the dc component and will be indicated with the uppercase letters hereafter. The phase-locked loop (PLL) aligns the d-axis component of the positive sequence voltage on $\bar{V}_g^+$, i.e.

$$V_{dg}^+ = \left|\bar{V}_g^+\right| \qquad V_{qg}^+ = 0 \tag{5}$$

The dq components of the negative sequence voltage are obtained from the properties of the decoupled PLL [27]:

$$\begin{aligned} V_{dg}^- &= real\left(\bar{V}_g^- / \exp\left[j \cdot \text{angle}\left(\bar{V}_g^+\right)\right]\right) \\ V_{qg}^- &= imag\left(\bar{V}_g^- / \exp\left[j \cdot \text{angle}\left(\bar{V}_g^+\right)\right]\right) \end{aligned} \tag{6}$$

where $real()$ and $imag()$ respectively represent the real and imaginary part of the complex number inside their brackets.

Let $\hat{I}_{dg}$ and $\hat{I}_{qg}$ be the d- and q-axis current outputs of the GSC to achieve the desired active and reactive power generation. By assuming the MPPT algorithm output is constant during short-circuit (i.e. no change in the active power received by the MSC), the desired d-axis current output of GSC can be approximated by

$$\hat{I}_{dg} = P'_g \Big/ V_{dg}^+ \tag{7}$$

where P'_g is the pre-fault active power output of the WTG.

The PI regulator of the WPC has a very slow response. Moreover, during severe voltage sags at the POI, its output $\Delta V'$ is frozen and its input ($Q'_{POI} - Q_{POI}$) is blocked to avoid overvoltage following the fault removal [15]. Hence, $\Delta V'$ is assumed to remain at its pre-fault value during short-circuit. The desired q-axis current output of GSC can be approximated by:

$$\hat{I}_{qg} = -K_V\left(1 + \Delta V' - \left|\bar{V}_g^+\right|\right) \tag{8}$$

The GSC current limits in (1) are accounted as below

$$I'_{dg} = \min\left(\hat{I}_{dg}, I_{dg}^{\lim}\right), \quad I_{dg}^{\lim} = 1\ pu$$
$$I'_{qg} = \min\left(\hat{I}_{qg}, I_{qg}^{\lim}\right), \quad I_{qg}^{\lim} = \sqrt{\left(I_g^{\lim}\right)^2 - \left(I'_{dg}\right)^2} \tag{9}$$

When the FRT function is active, the priority is given to the reactive current and GSC current limits become

$$I'_{qg} = \min\left(\hat{I}_{qg}, I_{qg}^{\lim}\right), \quad I_{qg}^{\lim} = 1\ pu$$
$$I'_{dg} = \min\left(\hat{I}_{dg}, I_{dg}^{\lim}\right), \quad I_{dg}^{\lim} = \sqrt{\left(I_g^{\lim}\right)^2 - \left(I'_{qg}\right)^2} \tag{10}$$

Ideally, the GSC with CSC is not expected to inject any negative sequence currents to the grid during unbalanced faults. Hence, the short circuit current contribution of the GSC with CSC can be written as below

$$\bar{I}_g^+ = \left(I'_{dg} + jI'_{qg}\right)\exp\left[j \cdot \text{angle}\left(\bar{V}_g^+\right)\right]$$
$$\bar{I}_g^- = 0 \tag{11}$$

When the GSC is operating under DSC, it injects negative sequence currents to eliminate the second harmonic oscillations in the GSC active power output (P_{C2} and P_{S2} in (3)). As the positive and negative sequence dq reference frame currents and voltages contain only the dc component in steady-state conditions, (3) - (4) can be written as below.

$$\begin{bmatrix} I_{qg}^{+\prime} \\ I_{dg}^{+\prime} \\ I_{qg}^{-\prime} \\ I_{dg}^{-\prime} \end{bmatrix} = \begin{bmatrix} 1 & 0 & 0 & 0 \\ V_{qg}^+ & V_{dg}^+ & V_{qg}^- & V_{dg}^- \\ V_{qg}^- & V_{dg}^- & V_{qg}^+ & V_{dg}^+ \\ -V_{dg}^- & V_{qg}^- & V_{dg}^+ & -V_{qg}^+ \end{bmatrix}^{-1} \begin{bmatrix} I'_{qg} \\ P_0 \\ P_{C2} \\ P_{S2} \end{bmatrix} \tag{12}$$

In phasor domain model, the d-axis current references are revised as below when $\left(\left|I_{dg}^{+\prime}\right| + \left|I_{dg}^{-\prime}\right|\right) > I_{dg}^{\lim}$.

$$I_{dg}^{+\prime\prime} = I_{dg}^{+\prime}\left[I_{dg}^{\lim} \Big/ \left(\left|I_{dg}^{+\prime}\right| + \left|I_{dg}^{-\prime}\right|\right)\right]$$
$$I_{dg}^{-\prime\prime} = I_{dg}^{-\prime}\left[I_{dg}^{\lim} \Big/ \left(\left|I_{dg}^{+\prime}\right| + \left|I_{dg}^{-\prime}\right|\right)\right] \tag{13}$$

The same principle applies for the q-axis current reference:

$$I_{qg}^{+\prime\prime} = I_{qg}^{+\prime}\left[I_{qg}^{\lim} \Big/ \left(\left|I_{qg}^{+\prime}\right| + \left|I_{qg}^{-\prime}\right|\right)\right]$$
$$I_{qg}^{-\prime\prime} = I_{qg}^{-\prime}\left[I_{qg}^{\lim} \Big/ \left(\left|I_{qg}^{+\prime}\right| + \left|I_{qg}^{-\prime}\right|\right)\right] \tag{14}$$

The short circuit current contribution of the GSC with DSC can be written as below.

$$\bar{I}_g^+ = \left(I_{dg}^{+\prime\prime} + jI_{qg}^{+\prime\prime}\right)\exp\left[j \cdot \text{angle}\left(\bar{V}_g^+\right)\right]$$
$$\bar{I}_g^- = \left(I_{dg}^{-\prime\prime} - jI_{qg}^{-\prime\prime}\right)\exp\left[j \cdot \text{angle}\left(\bar{V}_g^+\right)\right] \tag{15}$$

A. Alternative DSC Scheme

The Technical Connection Rules specified in VDE-AR-N 4120 [22] defines another behavior for the negative sequence system during unbalanced faults. The goal is to reduce the negative sequence voltage by consuming negative sequence reactive power. During FRT operation, the negative sequence reactive current is proportional to the voltage:

$$I_{qg}^{-\prime} = K_{neg}\left|\bar{V}_g^-\right| \tag{16}$$

where K_{neg} is the proportional gain between negative sequence voltage and reactive current, that varies between 2 and 6 as given in Fig. 4.

The positive sequence reactive current reference is calculated by the outer control proportional voltage regulator (see (8)), i.e.

$$I_{qg}^{+\prime} = \hat{I}_{qg} \tag{17}$$

The reactive current reference has to be revised using (14) when $\left(\left|I_{qg}^{+\prime}\right| + \left|I_{qg}^{-\prime}\right|\right) > I_{qg}^{\lim}$.

The positive sequence active current reference becomes

$$I_{dg}^{+\prime} = \hat{I}_{dg} \tag{18}$$

as there is no active power exchange on negative sequence, i.e.

$$I_{dg}^{-\prime} = 0 \tag{19}$$

As the priority is given to the reactive currents, positive sequence active current reference has to be revised considering the GSC current limit:

$$I_{dg}^{+\prime\prime} = \min\left(I_{dg}^{+\prime}, I_{dg}^{\lim}\right), I_{dg}^{\lim} = \sqrt{\left(I_g^{\lim}\right)^2 - \left(\left|I_{qg}^{+\prime\prime}\right| + \left|I_{qg}^{-\prime\prime}\right|\right)^2} \tag{20}$$

Note that, in this section, the negative sequence d and q components are defined based on the negative sequence voltage, i.e. $I_{dg}^{-\prime\prime}$ is in phase with $\bar{V}_g^-$ and $I_{qg}^{-\prime\prime}$ is 90° shifted compared to $\bar{V}_g^-$. The negative sequence current phasor is obtained with:

$$\bar{I}_g^- = \left(I_{dg}^{-\prime\prime} + jI_{qg}^{-\prime\prime}\right)\exp\left[j \cdot \text{angle}\left(\bar{V}_g^-\right)\right] \tag{21}$$

In the previous section, the negative sequence d and q components are defined based on the positive sequence voltage, i.e. $I_{dg}^{-\prime\prime}$ is in phase with $\bar{V}_g^+$.

The positive sequence current is calculated as:

$$\bar{I}_g^+ = \left(I_{dg}^{+\prime\prime} + jI_{qg}^{+\prime\prime}\right)\exp\left[j \cdot \text{angle}\left(\bar{V}_g^+\right)\right] \tag{22}$$

IV. Solution Algorithm

The phasor domain analysis is performed with the modified augmented nodal analysis (MANA) approach [30]. The resulting system of equations is represented by a sparse matrix that can be rapidly solved using sparse LU factorization algorithms. Switches in the system matrix represent the short circuit conditions for any type and number of simultaneous shunt or series faults [18]. Before applying a fault, the power network is converted into its linear equivalent based on load flow results. The Type-IV WTs except shunt harmonic ac filters are represented with current sources as shown in Fig. 7. $\bar{\mathbf{V}}_{abc,g}$ is the vector of GSC terminal voltages and $\bar{\mathbf{I}}_{abc,g}$ is the vector of GSC output currents in abc reference frame. $\bar{\mathbf{I}}_{abc,g}$ is calculated from the sequence components as:

$$\bar{\mathbf{I}}_{abc,g} = \begin{bmatrix} 1 \\ a^2 \\ a \end{bmatrix} \bar{I}_g^+ + \begin{bmatrix} 1 \\ a \\ a^2 \end{bmatrix} \bar{I}_g^- , \qquad a = \mathrm{e}^{j\frac{2\pi}{3}} \tag{23}$$

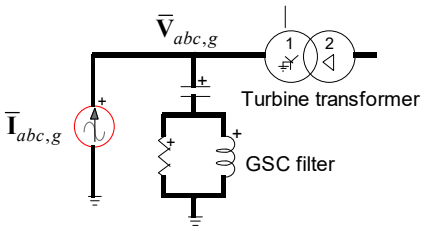

Fig. 7. Type-IV WTG current source phasor model.

The network is afterwards solved in phasor domain by applying the fault while keeping the WTG as a constant current source using pre-fault conditions. This solution provides the new voltage conditions in the network following the fault. According to the control mode and limiter constraints, and the new voltage conditions the WTG current is adjusted. In the system of equations **Ax = b**, the current sources are updated in the **b** vector. Consequently the **A** matrix stays constant and does not need re-factorization. This iterative solution is performed till convergence.

The detailed algorithm is given below.

$k = 0$

DO WHILE ($k <$ Nmax)

1. $k = k+1$
2. Solve network equations using $\bar{\mathbf{I}}_{abc,g}^{(k-1)}$
3. Calculate $\Delta V_g^{+(k)} = \left\| \bar{V}_g^{+(k)} \right| - \left| \bar{V}_g^{+(k-1)} \right\|$

   $\Delta V_g^{-(k)} = \left\| \bar{V}_g^{-(k)} \right| - \left| \bar{V}_g^{-(k-1)} \right\|$
4. *IF* $\left(\Delta V_g^{+(k)} < \varepsilon\right)$ *AND* $\left(\Delta V_g^{-(k)} < \varepsilon\right)$ *THEN*

   CONVERGED, $\bar{\mathbf{I}}_{abc,g}^{(k)} = \bar{\mathbf{I}}_{abc,g}^{(k-1)}$, *GO TO* Step-14
5. Calculate dq reference frame voltages (V_{dg}^+, V_{qg}^+, V_{dg}^- and V_{qg}^-) using (5) and (6)
6. Calculate the desired values for the d and q-axis GSC currents ($\hat{I}_{dg}$ and $\hat{I}_{qg}$) using (7) and (8), respectively
7. *IF (*Normal Operation*) THEN*

   Calculate the reference values for the d and q-axis GSC currents (I'_{dg} and I'_{qg}) using (9)

   ELSE (i.e FRT Operation)

   Calculate the reference values for the d and q-axis GSC currents (I'_{dg} and I'_{qg}) using (10)

   END IF
8. *IF* coupled sequence control *THEN*

   Calculate the short circuit current contribution of the GSC using (11) and *GO TO* Step-13
9. Calculate the reference values produced by the decoupled sequence current controller ($I_{dg}^{+\prime}$, $I_{qg}^{+\prime}$, $I_{dg}^{-\prime}$ and $I_{qg}^{-\prime}$) using (12)
10. *IF* $\left(I_{qg}^{+\prime} + I_{qg}^{-\prime}\right) > I_{qg}^{\lim}$ *THEN*

    Calculate revised q-axis reference currents ($I_{qg}^{+\prime\prime}$ and $I_{qg}^{-\prime\prime}$) using (14)

    ELSE (i.e. no limit violation)

    $I_{qg}^{+\prime\prime} = I_{qg}^{+\prime}$ and $I_{qg}^{-\prime\prime} = I_{qg}^{-\prime}$

    ENDIF
11. *IF* $\left(I_{dg}^{+\prime} + I_{dg}^{-\prime}\right) > I_{dg}^{\lim}$ *THEN*

    Calculate revised d-axis reference currents ($I_{dg}^{+\prime\prime}$ and $I_{dg}^{-\prime\prime}$) using (13)

    ELSE (i.e. no limit violation)

    $I_{dg}^{+\prime\prime} = I_{dg}^{+\prime}$ and $I_{dg}^{-\prime\prime} = I_{dg}^{-\prime}$

    ENDIF
12. Calculate the short circuit current contribution of the GSC using (15)
13. Update $\bar{\mathbf{I}}_{abc,g}^{(k)}$ using (23) for the next iteration
14. *IF (*CONVERGED for all WTs*) THEN EXIT*

END DO

In the algorithm above, k is the iteration number and Nmax is the maximum number of iterations. The pre-fault WTG voltages and currents are available from the load-flow solution.

The solution algorithm above is performed twice. The first solution is obtained with normal operation of WTGs in order to identify the GSCs that needs to be switched to FRT operation. In the second solution, the WTGs subjected to severe voltage sags in the first solution (i.e. $\left\| \bar{V}_m^+ \right| - 1 \left| > V_{FRT-ON} \right.$) operate in FRT mode.

When the negative sequence scheme of Section III.A is used for FRT operation, the above algorithm can be used after following modifications:

- Step-9: The initial reference values for the decoupled sequence currents will be calculated using (16) - (19) (for $I_{qg}^{-\prime}$, $I_{qg}^{+\prime}$, $I_{dg}^{+\prime}$ and $I_{dg}^{-\prime}$, respectively);
- Step-11: The revised d-axis positive sequence reference current ($I_{qg}^{+\prime\prime}$) will be calculated using (20);
- Step-12: The short circuit current contribution of the GSC will be calculated using (21) and (22).

V. Simulations

A. 120 kV Test System

Fig. 8 depicts the single-line diagram of the considered 120 kV, 60 Hz test system. The WP consists of 45 identical Type-VI WTGs with 1.5 MW rating. All WTGs are in service and operating under nominal wind speed (i.e. full load). The WP is operating with unity power factor (i.e. $Q_{POI} = 0$). Reader should refer to [15] for both wind park model and 120 kV test system details. EMTP [31] is used for EMT simulations. The WTG

converters are represented with the average value model.

Line-to-line-to-ground (LLG) and single-line-to-ground (SLG) faults are simulated at each 120 kV bus with 10^{-4} convergence tolerance. Due to space limitations, only the results at BUS1, BUS4 and BUS6 are presented here.

As seen from Table I - Table III the GSC operating under CSC injects a very small amount of negative sequence currents (EMTP solution) to the grid during LLG faults. Hence ignoring the negative sequence current contribution of the WTG (see equation (11)) does not cause a significant deterioration in the proposed phasor domain model accuracy. It should be noted that similar behavior is observed in SLG fault simulations (not presented in the paper). In Table I to Table III, and hereafter, the GSC voltage and current phasor magnitudes are given in pu and phase angle is given in degrees (format: magnitude (angle)).

The phasor and EMTP solutions are also compared for the GSC operating under DSC in Table I to Table III. The comparison for SLG fault simulations are presented in Table IV for the DSC scenario. The presented results in those tables confirm the accuracy of the proposed phasor model. As shown in Table V, the simulation errors in GSC positive and negative sequence current phasor magnitudes are less than 0.5% and 2.5%, respectively, in all presented simulation scenarios. The absolute difference between phasor and EMTP solution is less than 0.007 pu. It should be noted that, the simulation accuracy is better for the CSC scenarios when the simulation errors in GSC positive sequence current phasor magnitudes are considered.

Except the BUS1 fault scenarios (i.e. faults at POI), the tolerance is reached in less than 10 iterations in all simulations. The tolerance is reached at 13th iteration in both BUS1 LLG and SLG fault scenarios.

Table I: 120 kV System, LLG Fault at BUS1, DSC and CSC scenarios

GSC variable	DSC		CSC	
	EMTP-RV	Phasor Solution	EMTP-RV	Phasor Solution
$\bar{I}_g^+$	0.980 (-69.4)	0.983 (-68.1)	1.100 (-45.6)	1.100 (-46.7)
$\bar{V}_g^+$	0.482 (7.2)	0.484 (7.8)	0.496 (19.2)	0.500 (18.7)
$\bar{I}_g^-$	0.234 (-4.2)	0.239 (-3.3)	0.005 (-45.6)	0 (x)
$\bar{V}_g^-$	0.269 (-120.9)	0.270 (-121.0)	0.318 (-113.5)	0.321 (-113.8)

Table II: 120 kV System, LLG Fault at BUS4, DSC and CSC scenarios

GSC variable	DSC		CSC	
	EMTP-RV	Phasor Solution	EMTP-RV	Phasor Solution
$\bar{I}_g^+$	0.893 (-8.6)	0.893 (-8.5)	1.074 (0.6)	1.074 (0.7)
$\bar{V}_g^+$	0.812 (16.3)	0.812 (16.4)	0.804 (22.0)	0.804 (22.1)
$\bar{I}_g^-$	0.228 (26.5)	0.228 (26.5)	0.009 (57.4)	0 (x)
$\bar{V}_g^-$	0.201 (-136.0)	0.201 (-136.0)	0.243 (-119.6)	0.243 (-119.0)

Table III: 120 kV System, LLG Fault at BUS6, DSC and CSC scenarios

GSC variable	DSC		CSC	
	EMTP-RV	Phasor Solution	EMTP-RV	Phasor Solution
$\bar{I}_g^+$	0.990 (10.3)	0.992 (9.3)	1.003 (11.0)	0.999 (9.5)
$\bar{V}_g^+$	0.930 (19.4)	0.936 (19.3)	0.927 (19.7)	0.936 (19.5)
$\bar{I}_g^-$	0.051 (82.9)	0.050 (81.8)	0.001 (158.4)	0 (x)
$\bar{V}_g^-$	0.047 (-88.8)	0.047 (-88.5)	0.055 (-71.3)	0.055 (-71.0)

Table IV: 120 kV System, SLG Fault Scenarios with DSC

GSC variable	BUS1		BUS4		BUS6	
	EMTP-RV	Phasor Solution	EMTP-RV	Phasor Solution	EMTP-RV	Phasor Solution
$\bar{I}_g^+$	0.893 (-21.9)	0.894 (-21.8)	0.940 (7.6)	0.943 (7.1)	0.943 (11.3)	0.944 (10.9)
$\bar{V}_g^+$	0.738 (14.0)	0.738 (14.1)	0.945 (16.2)	0.948 (16.2)	0.973 (16.4)	0.976 (16.4)
$\bar{I}_g^-$	0.515 (-47.8)	0.515 (-47.8)	0.103 (-31.1)	0.101 (-30.9)	0.061 (22.7)	0.060 (21.8)
$\bar{V}_g^-$	0.320 (164.2)	0.320 (164.3)	0.099 (158.8)	0.099 (159.1)	0.063 (-153.0)	0.062 (-152.8)

Table V: 120 kV System Simulation Errors with DSC

Fault Location	LLG Fault		SLG Fault	
	$\lvert\bar{I}_g^+\rvert$	$\lvert\bar{I}_g^-\rvert$	$\lvert\bar{I}_g^+\rvert$	$\lvert\bar{I}_g^-\rvert$
BUS-1	0.3%	2.1%	0.1%	0.0%
BUS-4	0.0%	0.0%	0.4%	1.9%
BUS-6	0.2%	2.0%	0.1%	1.6%

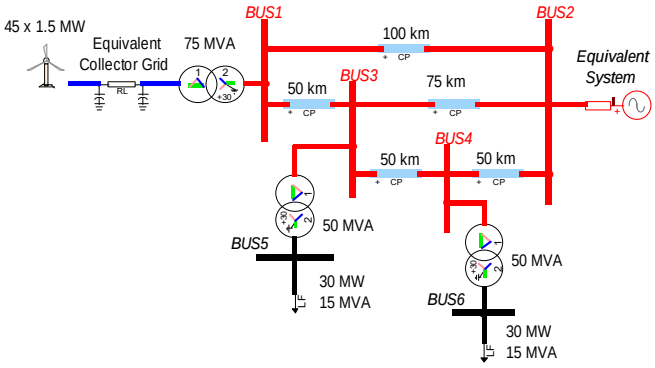

Fig. 8. 120 kV single wind park test system.

B. IEEE 39 Bus Test System

The considered multi wind park test system is shown in Fig. 9. This test system is obtained from IEEE 39 bus system by replacing two of the thermal power plants with wind parks [9]. Each wind park contains an aggregated model of 1.5 MW, 60 Hz Type-IV WTs, which is also used in the 120 kV test system. Both wind parks are operating at its full load (i.e. under nominal wind speed) with unity power factor (i.e. $Q_{POI} = 0$). Reader should refer to [9] for system details.

SLG and LLG faults are simulated at each 345 kV bus for both WTG CSC and DSC schemes with 10^{-4} convergence tolerance. However, only the results for the faults at F1, F2 and F3 are presented for the DSC scenarios in Table VI - Table XI

due to space limitations. The presented results in those tables confirm the accuracy. As shown in Table XII, the simulation errors in GSC positive and negative sequence current phasor magnitudes are less than 1% and 6%, respectively, in all presented simulation scenarios. The absolute difference between phasor and EMTP solution is below 0.007 pu. It should be noted that, the simulation accuracy is better for the CSC scenarios when the simulation errors in GSC positive sequence current phasor magnitudes are considered (not presented here).

The convergence characteristics is similar to the 120 kV test case. The phasor solution requires less than 10 iterations when the fault takes place on a bus without wind generation. For the faults at the POI of a wind park, on the other hand, the tolerance is reached in less than 14 iterations for the faults.

Table XIII shows the results obtained using the negative sequence scheme postulated in the VDE Technical Requirements for the LLG fault scenario at F1. The gain in Fig. 4 is taken as equal to 2. The EMTP model is modified considering the additional reactive current curve in Fig. 4, and the phasor model is built using the equations in Section III. A. As suggested by the results, the EMTP model is precisely represented in steady-state with the proposed steady-state methodology and phasor model.

Table VI: IEEE 39 Bus System, LLG Fault at F1, DSC Scenario

FC variable	WP1		WP2	
	EMTP-RV	Phasor Solution	EMTP-RV	Phasor Solution
$\bar{I}_g^+$	0.912 (-12.9)	0.913 (-12.9)	0.935 (-13.8)	0.936 (-13.9)
$\bar{V}_g^+$	0.823 (9.7)	0.823 (9.6)	0.837 (6.5)	0.838 (6.4)
$\bar{I}_g^-$	0.202 (4.3)	0.200 (4.0)	0.175 (10.5)	0.174 (10.2)
$\bar{V}_g^-$	0.176 (-156.7)	0.176 (-156.7)	0.152 (-152.9)	0.153 (-152.9)

Table VII: IEEE 39 Bus System, SLG Fault at F1, DSC Scenario

FC variable	WP1		WP2	
	EMTP-RV	Phasor Solution	EMTP-RV	Phasor Solution
$\bar{I}_g^+$	0.967 (-1.7)	0.964 (-2.5)	0.982 (-3.2)	0.978 (-3.9)
$\bar{V}_g^+$	0.941 (7.0)	0.945 (6.7)	0.939 (5.1)	0.943 (4.8)
$\bar{I}_g^-$	0.114 (74.6)	0.108 (73.7)	0.098 (78.5)	0.095 (78.1)
$\bar{V}_g^-$	0.106 (-98.3)	0.106 (-97.2)	0.091 (-94.1)	0.091 (-93.2)

Table VIII: IEEE 39 Bus System, LLG Fault at F2, DSC Scenario

FC variable	WP1		WP2	
	EMTP-RV	Phasor Solution	EMTP-RV	Phasor Solution
$\bar{I}_g^+$	0.945 (-8.5)	0.947 (-8.3)	0.930 (-13.7)	0.931 (-13.2)
$\bar{V}_g^+$	0.854 (9.9)	0.852 (9.9)	0.825 (9.1)	0.823 (9.1)
$\bar{I}_g^-$	0.159 (5.9)	0.161 (5.7)	0.180 (4.4)	0.181 (4.4)
$\bar{V}_g^-$	0.142 (-157.5)	0.142 (-157.8)	0.157 (-155.9)	0.157 (-156.1)

Table IX: IEEE 39 Bus System, SLG Fault at F2, DSC Scenario

FC variable	WP1		WP2	
	EMTP-RV	Phasor Solution	EMTP-RV	Phasor Solution
$\bar{I}_g^+$	0.959 (-1.1)	0.952 (-1.8)	0.966 (-3.6)	0.968 (-4.2)
$\bar{V}_g^+$	0.949 (6.9)	0.953 (6.5)	0.929 (6.0)	0.933 (5.8)
$\bar{I}_g^-$	0.098 (72.0)	0.097 (71.2)	0.117 (72.2)	0.113 (71.5)
$\bar{V}_g^-$	0.096 (-100.9)	0.097 (-100.5)	0.106 (-99.8)	0.107 (-99.3)

Table X: IEEE 39 Bus System, LLG Fault at F3, DSC Scenario

FC variable	WP1		WP2	
	EMTP-RV	Phasor Solution	EMTP-RV	Phasor Solution
$\bar{I}_g^+$	0.921 (0.8)	0.913 (0.1)	0.954 (-0.9)	0.947 (-1.7)
$\bar{V}_g^+$	0.976 (5.8)	0.979 (5.4)	0.959 (5.3)	0.963 (5.0)
$\bar{I}_g^-$	0.044 (4.1)	0.043 (4.0)	0.052 (4.3)	0.051 (3.7)
$\bar{V}_g^-$	0.046 (-170.8)	0.046 (-170.7)	0.052 (-169.6)	0.052 (-169.7)

Table XI: IEEE 39 Bus System, SLG Fault at F3, DSC Scenario

FC variable	WP1		WP2	
	EMTP-RV	Phasor Solution	EMTP-RV	Phasor Solution
$\bar{I}_g^+$	0.887 (1.5)	0.884 (1.3)	0.913 (-0.1)	0.911 (-0.4)
$\bar{V}_g^+$	1.005 (3.4)	1.007 (3.2)	0.992 (2.8)	0.994 (2.6)
$\bar{I}_g^-$	0.021 (70.9)	0.021 (70.8)	0.025 (71.2)	0.025 (71.1)
$\bar{V}_g^-$	0.024 (-107.1)	0.024 (-107.3)	0.027 (-105.8)	0.027 (-105.9)

Table XII: IEEE 39 Bus System Simulation Errors for DSC Scenarios

Fault Type	Fault Location	WP1		WP2	
		$\lvert\bar{I}_g^+\rvert$	$\lvert\bar{I}_g^-\rvert$	$\lvert\bar{I}_g^+\rvert$	$\lvert\bar{I}_g^-\rvert$
LLG	F1	0.1%	1.0%	0.1%	0.6%
	F2	0.2%	1.3%	0.1%	0.6%
	F3	0.9%	2.3%	0.7%	1.9%
SLG	F1	0.3%	5.3%	0.4%	3.1%
	F2	0.7%	1.0%	0.2%	3.4%
	F3	0.3%	0.0%	0.2%	0.0%

Table XIII: IEEE 39 Bus System, LLG Fault at F1, VDE DSC Scenario

FC variable	WP1 (VDE DSC)		WP2 (VDE DSC)	
	EMTP-RV	Phasor Solution	EMTP-RV	Phasor Solution
$\bar{I}_g^+$	0.842 (-16.5)	0.842 (-16.6)	0.879 (-16.2)	0.879 (-16.3)
$\bar{V}_g^+$	0.826 (7.8)	0.827 (7.7)	0.841 (5.0)	0.841 (4.9)
$\bar{I}_g^-$	0.257 (-46.6)	0.258 (-46.8)	0.221 (-43.0)	0.221 (-43.2)
$\bar{V}_g^-$	0.129 (-136.6)	0.129 (-136.8)	0.110 (-133.0)	0.111 (-133.2)

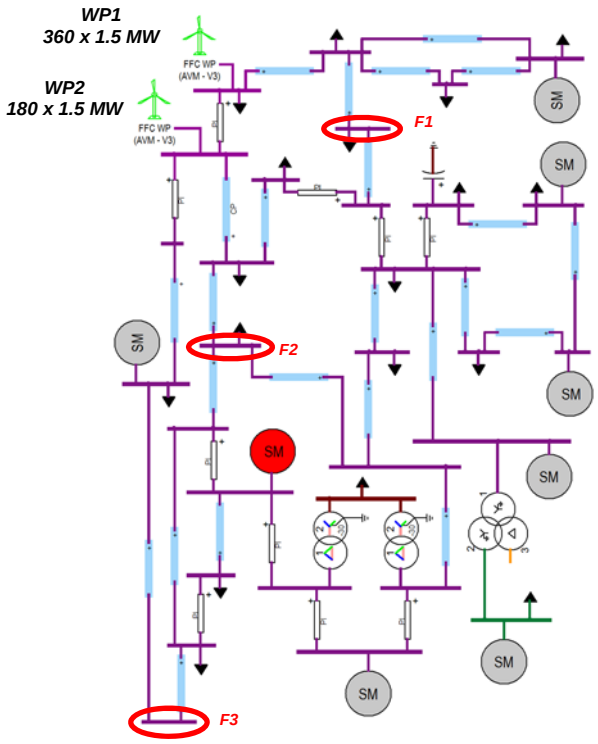

Fig. 9. IEEE 39 Bus multi wind park test system.

VI. Conclusion

This paper presented an accurate phasor domain model of Type-IV WTG for short circuit analysis. The proposed model uses the concept of control based equivalent circuits and accounts for the GSC control through an iterative loop solution. The GSC control includes fault-ride-through function and the option of decoupled sequence control scheme. The model is incorporated into an MANA based multiphase short circuit solver and validated by comparisons with the EMT simulations.

The accuracy of the proposed model is tested by simulating various unbalanced faults on two separate test systems: 120 kV single wind park test system and IEEE 39 Bus multi wind park test system. The EMT simulation results are taken as reference solution. In all simulations, the difference between the phasor domain and EMT solutions are less than 0.007 pu when the GSC positive and negative sequence current phasor magnitudes are considered. The presented simulation results also confirms that the proposed modeling approach has the ability to represent Type-IV WTGs with different control schemes.

References

[1] E. Muljadi and V. Gevorgian, "Short-Circuit Modelling of a Wind Power Plant," *Proc. 2011 IEEE PES General Meeting*, Detroit, MI, July 24-29, 2011.

[2] J. Martinez, P. C. Kjar, P. Rodriguez, and R. Teodorescu, "Short Circuit Signatures from Different Wind Turbine Generator Types," *Proc. 2011 IEEE Power Systems Conf. and Expo*, Phoenix, AZ, Mar. 20-23, 2011.

[3] R. A. Walling, E. Gursoy, and B. English, "Current Contribution from Type 3 and Type 4 Wind Turbine Generators During Faults," *Proc. 2011 IEEE PES General Meeting*, Detroit, MI, July 24-29, 2011.

[4] E. Farantatos, U. Karaagac, H. Saad and J. Mahseredjian, "Short-Circuit Current Contribution of Converter Interfaced Wind Turbines and the Impact on System Protection," in *Proc. Bulk Power Systems Dynamics and Control - IX (IREP)*, Rethymnon, Crete, Greece, Aug. 25-30, 2013.

[5] H. Hooshyar, and M. E. Baran, "Fault Analysis on Distribution Feeders with High Penetration of PV Systems," *IEEE Trans. Power Systems*, vol. 28, no.3, August 2013.

[6] "Grid code - high and extra high voltage," E.ON Netz GmbH, Bayreuth, Germany, April 2006.

[7] D. F. Howard, "Short Circuit Currents in Wind-Turbine Generator Networks", Ph.D. Thesis in Electrical and Computer Engineering, Georgia Institute of Technology, Dec. 2013.

[8] M. Fischer and A. Mendonca, "Representation of Variable Speed Full Conversion Wind Energy Converters for Steady-State Short Circuit Calculations," in Proc. IEEE PES Transmission & Distribution Conference & Exposition, Orlando, FL, May 7-10, 2012.

[9] U. Karaagac, T. Kauffmann, I. Kocar, H. Gras, J. Mahseredjian and F. Farantatos, "Phasor domain modeling of Type IV wind turbine generator for protection studies," *Proc. 2015 IEEE PES General Meeting*, Denver, CO, 26-30 July 2015.

[10] Impact of Renewables on System Protection: Wind/PV Short-Circuit Phasor Model Library and Guidelines for System Protection Studies. EPRI, Palo Alto, CA: 2016, 3002008367.

[11] I. Erlich, T. Neumann, F. Shewaega, P. Schegner and J. Meyer, "Wind Turbine Negative Sequence Current Control and its Effect on Power System Protection," *Proc. 2013 IEEE PES General Meeting*, Vancouver, BC, July 21-25, 2013.

[12] M. Nagpal and C. Henville, "Impact of Power-Electronic Sources on Transmission Line Ground Fault Protection", IEEE Trans. Power Del., vol. 33, no. 1, pp. 62–70, February 2018.

[13] "Impact of Inverter Based Generation on Bulk Power System Dynamics and Short-Circuit Performance", PES-TR68, IEEE/NERC Task Force on Short-Circuit and System Performance Impact of Inverter Based Generation, July 2018.

[14] R. Teodorescu, M. Liserre, P. Rodriguez, *Grid Converters for Photovoltaic and Wind Power Systems*, IEEE-Wiley, 2011.

[15] U. Karaagac, J. Mahseredjian, H. Gras, H. Saad, J. Peralta and L. D. Bellomo, "Simulation Models for Wind Parks with Variable Speed Wind Turbines in EMTP-RV", research report, Polytechnique Montréal, December 2016.

[16] T. Kauffmann, U. Karaagac, I. Koçar, S. Jensen, J. Mahseredjian, E. Farantatos, "An Accurate Type III Wind Turbine Generator Short Circuit Model for Protection Applications," *IEEE Trans. Power Delivery*, vol. 32, no. 6, pp. 2370-2379, December 2017.

[17] I. Kocar, J. Mahseredjian, U. Karaagac, G. Soykan and O. Saad, "Multiphase Load Flow Solution of Large Scale Distribution Systems using the Concept of Augmented Matrices," *IEEE Trans. Power Delivery*, vol. 29, no. 2, April 2014.

[18] I. Kocar, J. S. Lacroix, F. Therrien, "General and simplified computation of fault flow and contribution of distributed sources in unbalanced distribution networks", *Proc. of IEEE PES General Meeting*, 2012.

[19] A. Haddadi, I. Kocar, T. Kauffmann, U. Karaagac, E. Farantatos, and J. Mahseredjian, "Field validation of generic wind park models using fault records," submitted to *Journal of Modern Power System and Clean Energy*, November 2018.

[20] Impact of Renewables on System Protection: Wind/PV Short-Circuit Phasor Model Library and Guidelines for System Protection Studies, EPRI, Palo Alto, CA: 2016. 3002008367.

[21] Short-Circuit Phasor Models of Inverter-Based Resources for Fault Studies - Model Validation Case Studies, EPRI, Palo Alto, CA: 2018, 3002013634.

[22] Technische Regeln für den Anschluss von Kundenanlagen an das Hochspannungsnetz und deren Betrieb (TAR Hochspannung), VDE-AR-N 4120 Anwendungsregel: 2018-11.

[23] V. Akhmatov, A. H. Nielsen, J. K. Pedersen, O. Nymann, "Variable-speed wind turbines with multi-pole synchronous permanent magnet generators. Part I: Modelling in dynamic simulation tools", *Wind Eng.*, vol. 27, no. 6, pp. 531-548, Dec. 2003.

[24] J. M. Garcia, "Voltage control in wind power plants with doubly fed generators," Ph.D. thesis, Alaborg Univ., Denmark, Sep. 2010.

[25] U. Karaagac, H. Saad, J. Peralta, J. Mahseredjian, "Simulation models for wind parks with variable speed wind turbines in EMTP-RV", April 2016, Polytechnique Montréal.

[26] P. Rodriguez , J. Pou , J. Bergas , J.I. Candela , R.P. Burgos and D. Boroyevich, "Double synchronous reference frame PLL for power converters", Proc. IEEE PESC, pp. 1415-1421, 2005.

[27] P. Rodriguez , J. Pou , J. Bergas , J.I. Candela , R.P. Burgos and D. Boroyevich, "Decoupled Double Synchronous Reference Frame PLL for

Power Converters Control", *IEEE Trans. Power Electronics*, 22,March 2007, 584–592.

[28] J. M. Garcia, "Voltage control in wind power plants with doubly fed generators," Ph.D. thesis, Alaborg Univ., Denmark, Sep. 2010.

[29] R. Teodorescu, M. Liserre, P. Rodriguez, Grid Converters for Photovoltaic and Wind Power Systems, 2011, IEEE/Wiley.

[30] J. Mahseredjian and F. Alvarado, "Creating an Electromagnetic Transients Program in MATLAB: MatEMTP," *IEEE Trans. Power Delivery*, January 1997, vol. 12, pp 380-388.

[31] J. Mahseredjian, S. Dennetière, L. Dubé, B. Khodabakhchian and L. Gérin-Lajoie, "On a New Approach for the Simulation of Transients in Power Systems". *Electric Power Systems Research*, vol. 77, issue 11, September 2007, pp. 1514-1520.